scientific reports

Check for updates

OPEN

Reinforcement of impaired shield tunnel structure by stainless steel corrugated plate

Yimin Qin[1], Yizheng Chen[2]✉, Yan Tang[2], Cheng Zhong[3], Shurong Li[3] & Xian Liu[1]✉

This paper presents a case study on the reinforcement of an impaired shield tunnel structure using Stainless Steel Corrugated Plate (SSCP) in China. The SSCP used in this study is made from the novel duplex stainless steel S32001, characterized by its high strength, light weight, and corrosion resistance. A full-scale test is conducted to investigate the mechanical behavior of the SSCP-reinforced tunnel structure. Experimental results reveal that SSCP reinforcement significantly enhances structural bearing capacity and stiffness, with shear failure at the bonding interface identified as the primary failure mode. Based on these findings, two design concepts are proposed: enhancing interface bonding shear strength and improving connecting stiffness between SSCPs. The practical application of SSCP reinforcement in the case study tunnel is then carried out, where the design concepts are successfully applied. Additionally, the practical implementation also reveals that SSCP reinforcement offers superior construction and economic efficiency compared to traditional steel plate reinforcement. This study provides valuable insights into both academic research and engineering practice, demonstrating the potential of SSCP as an effective solution for reinforcing impaired shield tunnels.

Keywords Shield tunnel, Stainless steel corrugated plate, Full-scale test, Strengthening techniques, Bearing capacity, Case study

The mileage of shield tunnel subway lines in mainland China reaches 8,548 km by the end of 2023[1]. Inspections, both manual[2–4] and automated[5–7], detect several deteriorated shield tunnel structures. With the increase in mileage, the number of deteriorated shield tunnels rises, drawing additional attention to reinforcement efforts in both academic and engineering fields[8,9].

The primary objective of reinforcing impaired subway shield tunnels is to enhance their bearing capacity and stiffness within a limited construction timeframe[10]. Due to the high utility rate of subway tunnels, only a few hours each night are available for reinforcement construction. Researchers and engineers are collaborating to develop better solutions for shield tunnel reinforcement. Researchers focus on inventing novel reinforcement technology[10–13], investigating their reinforcing benefits and failure mechanisms[14,15], and proposing applicable design theories[16,17]. Engineers concentrate on developing functional equipment and feasible construction methods for efficient practical implementation[18,19].

Recently, a new stainless steel corrugated plate (SSCP) S32001 is manufactured (Fig. 1). The SSCP has a thickness of 6 mm, a width of 460 mm, and an arc length of either 1197.1or 1354.7 mm. It features a sinusoidal wave pattern with a height of 51.2 mm from crest to trough, providing high stiffness transverse to the corrugation direction. An overlap section with an arc length of 76.5 mm is designed for easy bolt connection between adjacent SSCPs, facilitated by the differing widths and heights at each end of the SSCP.

Made from the new duplex stainless steel S32001, the SSCP has a yield strength of 509 MPa at a plastic strain of 0.2%[20]. Each SSCP weighs about 40 kg. For long-term performance, research has demonstrated the durability and stability of S32001. Its corrosion resistance has been evaluated in a 3.5% NaCl solution through corrosion rate measurements, where S32001 exhibits a low corrosion rate of 0.1 $\mu A/cm^2$, indicating passive behavior with minimal corrosion activity over time[21]. Additionally, the fatigue performance of S32001 is confirmed through fatigue testing, showing superior fatigue strength compared to conventional threaded rods and rebars[22]. In comparison, conventional steel plates typically have a yield strength of 235 MPa[14], a weight of around 386 kg[23], and a corrosion rate of approximately 1.1 $\mu A/cm$[24], indicating the distinct advantages of S32001 in high strength, light weight, and superior corrosion resistance. These studies highlight the potential of S32001 for use in shield tunnel structures, which are exposed to humid and vibrational environments.

[1]College of Civil Engineering, Tongji University, Shanghai 200092, China. [2]Technology and Application, State Grid Smart Grid Research Institute Co., Ltd, Beijing 102209, China. [3]State Grid Hebei Electric Power Co., Ltd, Shijiazhuang 050081, China. ✉email: ycng828@hotmail.com; xian.liu@tongji.edu.cn

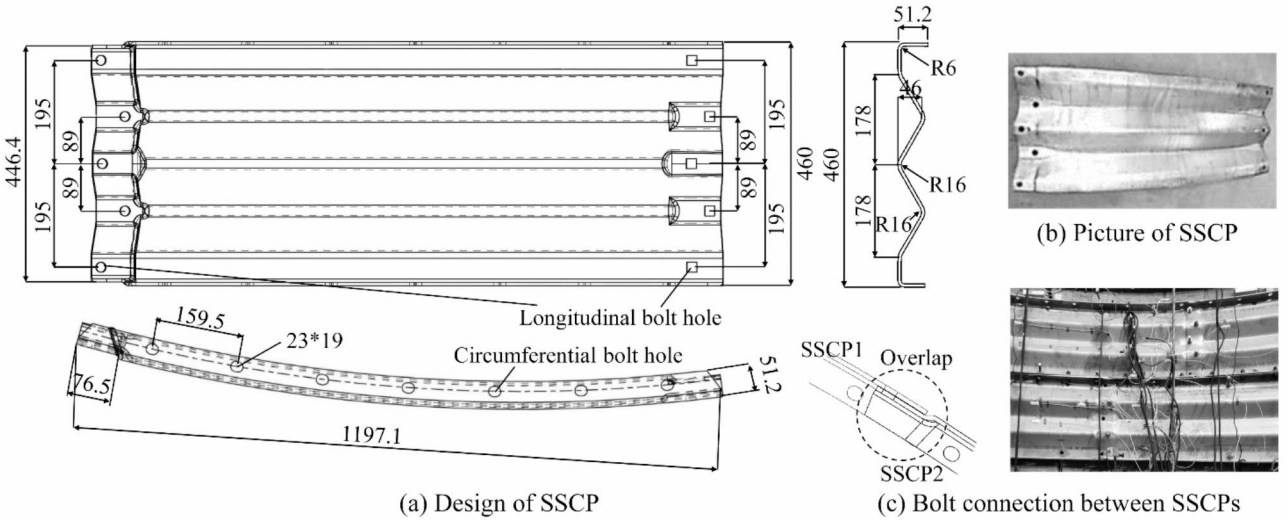

Fig. 1. Geometry and connection layout of SSCP.

Preliminary research suggests its potential application in tunnels[25]. The aforementioned material property tests show that SSCP exhibits promising strength, stiffness, and corrosion resistance. Additionally, pioneering experiments on the SSCP-reinforced beams prove their effectiveness in enhancing bearing capacity and stiffness[26–28]. From an engineering perspective, SSCP reinforcement is notably more constructible compared to the currently used epoxy-bonded steel plate method[19]. The light weight of SSCP allows for rapid transportation and easy assembly in tunnels, whereas the epoxy-bonded steel plate method requires large lifting machinery due to its relatively high weight. Adjacent SSCPs are connected by bolts rather than welding, which avoids the practical difficulties of ensuring quality in overhead welding. A challenge to the application of SSCP reinforcement is its height of 51.2 mm, which may be infeasible in tunnels with severe deformation and limited space. However, with the trend toward larger-diameter shield tunnels, particularly for river-crossing and sea-crossing projects, there is generally more space available within these tunnels. This trend indicates that SSCP reinforcement could be a viable solution for shield tunnel structures in such cases.

Furthermore, gaps remain between the research status and practical application:

(1) Academically, the mechanical behavior and failure mode of SSCP-reinforced shield tunnels are not fully studied. Recent studies overlook the comprehensive effects of segments and joints by conducting segment and joint tests separately[26–28]. Shield tunnels are assembled from precast concrete segments with natural longitudinal joints between them, and their mechanical behavior highly depends on the layout of these segments and joins[29,30]. Therefore, a full-ring test considering both the effects of segments and joins is indispensable for investigating the mechanical behavior and failure mode.
(2) The design concept, serving as a bridge between academia and engineering, is missing from previous research. It guides the identification of vulnerable positions where structural failure is likely to occur, enabling the predictive design of SSCP reinforcement.
(3) Practically, some pioneering application of SSCP is reported in the field of tunnel-supporting structures[31] and culverts[32]. However, there is no implementation of SSCP reinforcement in shield tunnel structures. Practical implementation is necessary to investigate constructability and establish the construction process for SSCP reinforcement, providing valuable experience for future applications.

To address the gaps, this paper presents a case study on the reinforcement of an impaired shield tunnel structure using SSCP. Firstly, a full-scale test is conducted to reveal the mechanical behavior and failure mode of SSCP-reinforced shield tunnels, considering the comprehensive effects of segments and joints. Secondly, design concepts are proposed based on the experimental observations. Finally, a practical implementation of SSCP reinforcement in a shield tunnel is reported, applying the proposed design concepts.

Site information of the impaired tunnel

Shield tunnel structure

Shield tunnels are constructed by precast concrete segments. Longitudinal and circumferential joints naturally form between segments[33], as illustrated in Fig. 2a, distinguishing shield tunnels from other tunnel structures.

The design of the case study tunnel is shown in Fig. 2b. The tunnel structure has an outer diameter of 8.5 m, an inner diameter of 7.7 m, and a width of 1.6 m. Each ring comprises seven concrete segments connected by two bolts at each longitudinal joint. Adjacent rings are connected by nineteen bolts at circumferential joints. These bolts have a grade of 6.8 and a diameter of 30 mm. The grade of the concrete is C55.

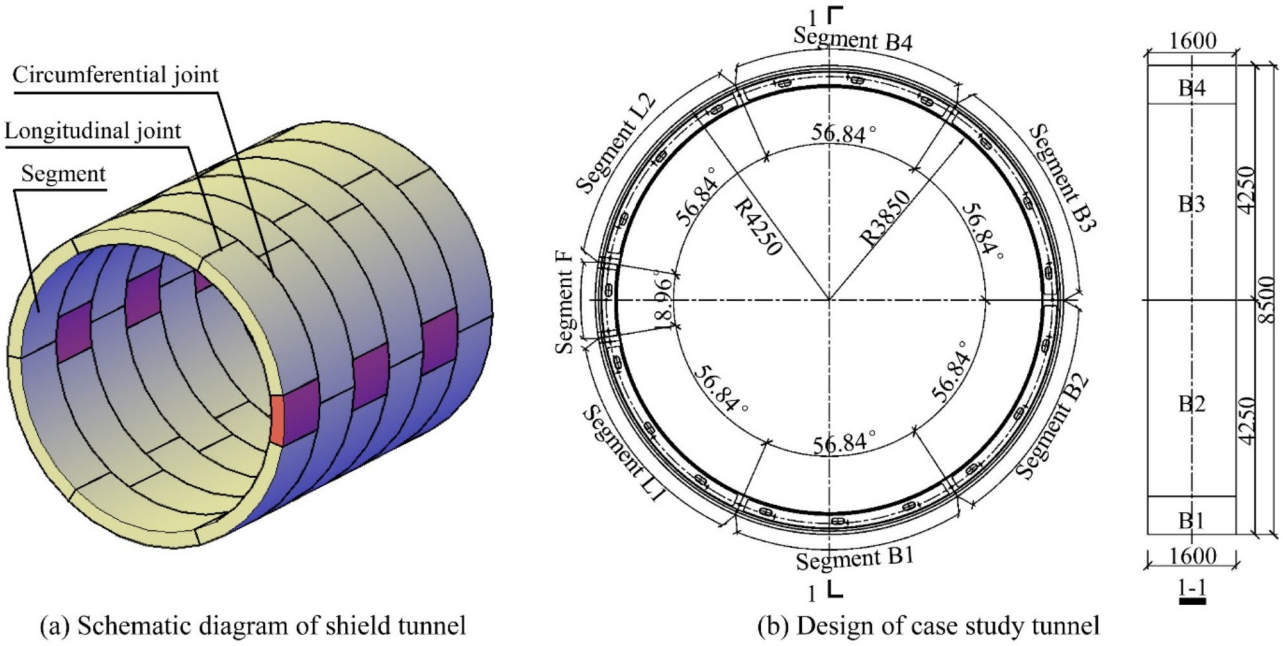

(a) Schematic diagram of shield tunnel (b) Design of case study tunnel

Fig. 2. Structural configuration of shield tunnel.

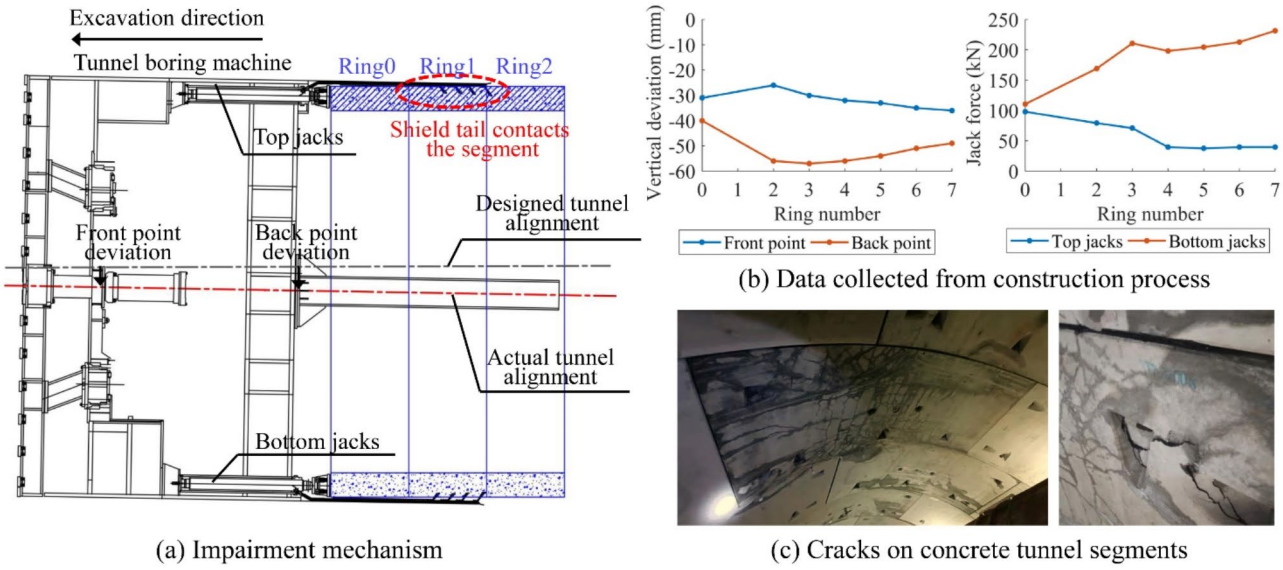

(a) Impairment mechanism (b) Data collected from construction process (c) Cracks on concrete tunnel segments

Fig. 3. Phenomenon and mechanism of impairment.

Construction-induced impairment

The tunnel boring machine (TBM) is essential in shield tunnel construction[34]. During excavation, the TBM advances by the width of one ring using jack forces. After each excavation, additional space in the shield tail allows for assembling a new ring. This process repeats throughout the construction.

In the case study, impairment occurs during construction, as shown in Fig. 3a. Vertical deviation measurements (Fig. 3b) reveal that the actual tunnel alignment is up to 56 mm lower than the design. To correct this, the bottom jack force is set to a high value of 200kN (Fig. 3b), causing a clockwise rotation of the TBM[35]. This upward movement reduces the alignment discrepancy. This rotation is significant since it decreases the vertical deviation by 20 mm over two-ring excavation. The significant rotation occupies the gap between the shield tail and tunnel structure, leading to a contact between the shield tail and concrete segments. The shield tail has high strength and stiffness and is made of a solid steel plate with a thickness of 50 mm. The contact causes cracks in the concrete segments (Fig. 3c).

Reinforcement is crucial for the safety of the impaired tunnel lining[36], presenting an opportunity for practical implementation of SSCP reinforcement.

Proposal of design concepts based on experimental observations

A full ring test is performed to uncover the reinforcing benefits and failure mechanism of SSCP-reinforced shield tunnel structures. Design concepts, that connect academic research with engineering practice, are proposed based on experimental observations.

Experimental program

Test specimen

Figure 4a shows the shield tunnel specimen, which has an outer diameter of 6.2 m and an inner diameter of 5.5 m. Each ring consists of six concrete segments, joined by two bolts at each longitudinal joint. Adjacent rings are connected by sixteen bolts at the circumferential joints. These bolts are grade 5.8 with a diameter of 30 mm. The grade of the concrete is C50. The specimen comprises three rings —upper, middle, and bottom ring— with widths of 0.6 m, 1.2 m and 0.6 m, respectively.

The specimen slightly differs from the case study tunnel described in the previous section due to the difficulty of obtaining the exact tunnel structure, which has an uncommon diameter. The 6.2 m outer diameter specimen was selected based on three key criteria for representativeness and feasibility. Failure mode similarity is prioritized, as failure mechanisms in reinforced tunnels rely primarily on the bonding interface rather than tunnel diameter, as demonstrated by comparative research[23]. Availability is also a factor, given that 6.2 m is a widely adopted size for shield tunnels in mainland China[37]. Finally, experimental feasibility is ensured, as the loading apparatus in this study can accommodate tunnels up to 6.9 m in diameter.

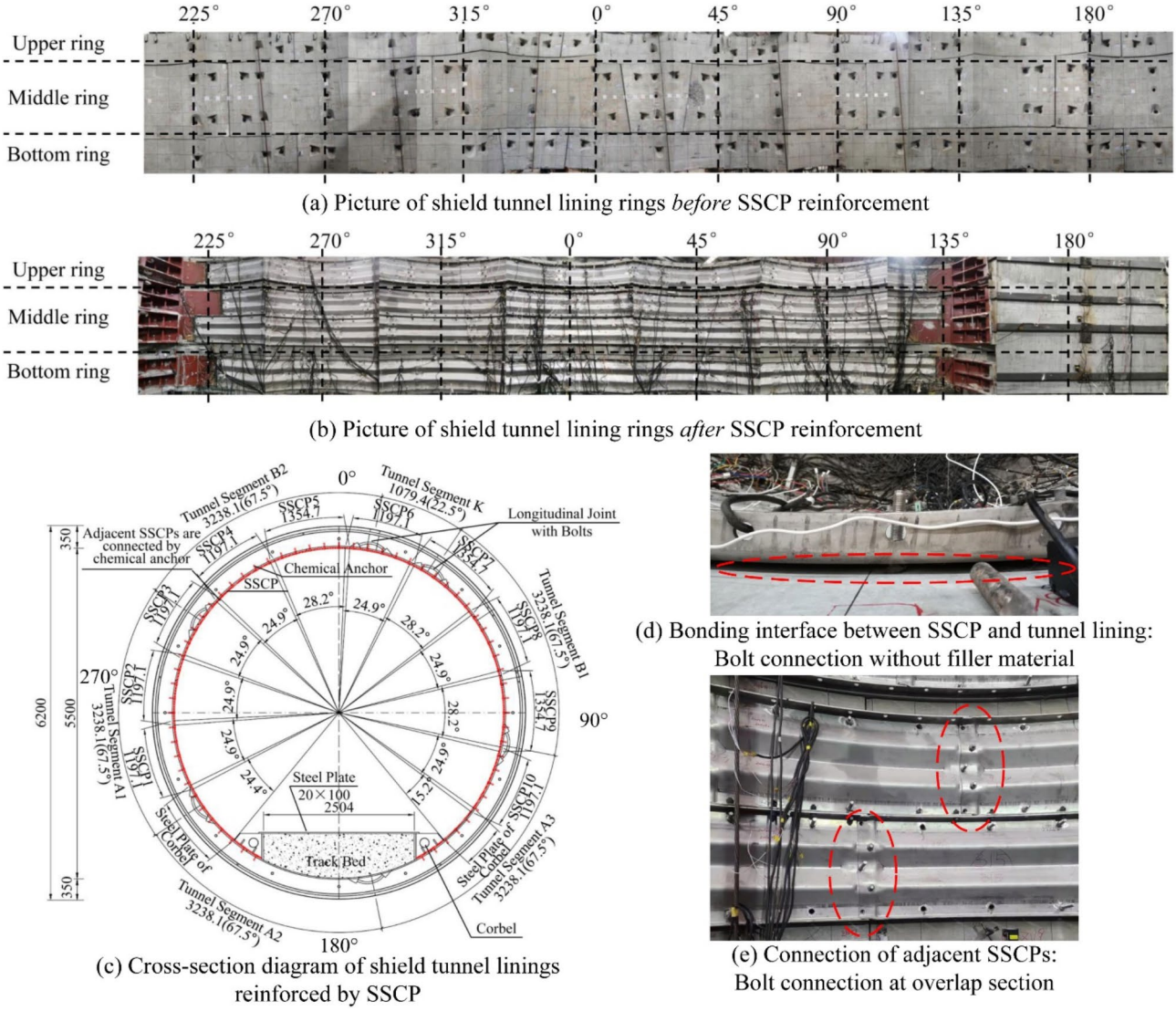

(a) Picture of shield tunnel lining rings *before* SSCP reinforcement

(b) Picture of shield tunnel lining rings *after* SSCP reinforcement

(c) Cross-section diagram of shield tunnel linings reinforced by SSCP

(d) Bonding interface between SSCP and tunnel lining: Bolt connection without filler material

(e) Connection of adjacent SSCPs: Bolt connection at overlap section

Fig. 4. Experiment specimen.

Material type	Young's modulus (N/mm^2)	Compressive strength (N/mm^2)	Yield stress (N/mm^2)
SSCP	2.06×10^5	/	490
Chemical anchor and bolt	2.06×10^5	/	640
Concrete	3.45×10^4	32.4	/

Table 1. Material properties.

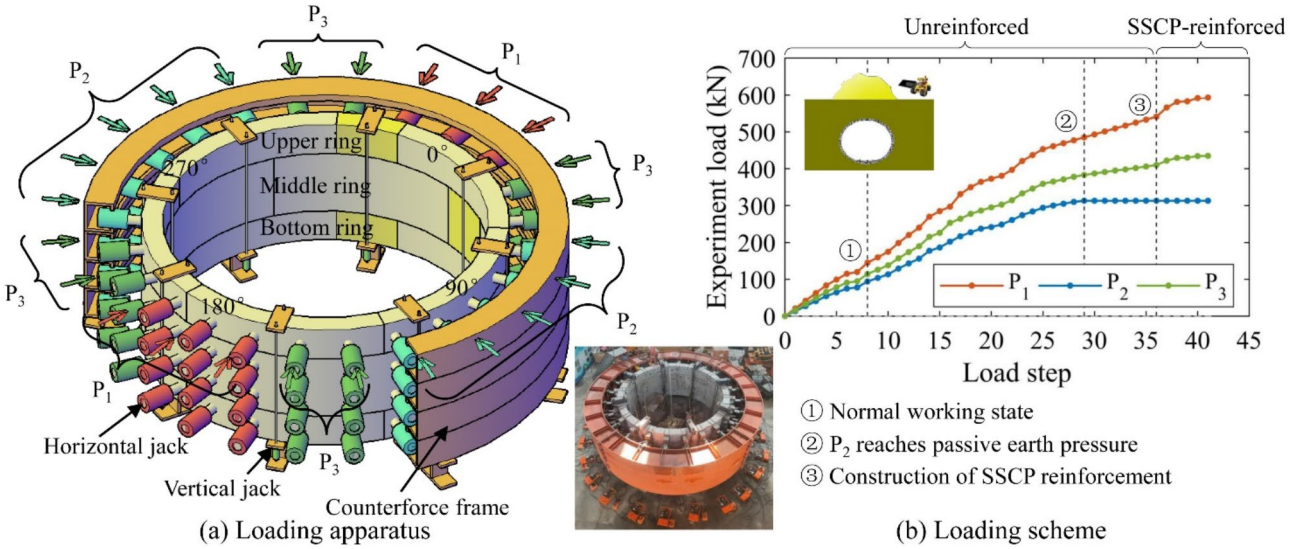

Fig. 5. Loading apparatus and scheme.

In terms of transferability to practical applications, the experimental results are adequate for evaluating the strengthening benefits, understanding the failure mechanisms, identifying vulnerable areas, and developing design concepts. Previous studies[23] have shown that reinforcement methods can be effective for tunnels of various sizes, as the strengthening benefits and failure mechanism remain consistent. Furthermore, the experimental results enable the identification of vulnerable areas within the SSCP-reinforced structure, offering design concepts for practical applications. Besides, to enhance the generalizability of the findings, additional tests on tunnels with varying diameters is suggested.

Figure 4b,c illustrate the SSCP reinforcement of the test specimen. The upper, middle, and bottom rings are reinforced with one, two, and one SSCP rings, respectively. Each SSCP ring comprises ten SSCPs, with material, geometry, and connections detailed in Fig. 1. These rings rest on the track bed, supported by steel corbels on both sides, which are connected by steel plates measuring 100 mm in width and 20 mm in thickness. The SSCP rings are anchored to tunnel lining using chemical anchors, each 190 mm long with an implantation length of 125 mm.

Figure 4d,e provide details of SSCP reinforcement. The bonding interface between the SSCP and tunnel lining relies on bolt connections without any filler material. Adjacent SSCPs within a ring are connected by three bolts at the overlap section, utilizing the longitudinal bolt holes of the SSCP. There is no connection between SSCP rings, as the circumferential bolt holes are not used in this experiment. Both bolts and anchors are made of 2205 stainless steel with a diameter of 16 mm. The material properties are listed in Table 1, according to the Chinese code[38,39].

Loading apparatus and scheme

A counterforce frame equipped with ninety-six hydraulic jacks serves as the loading apparatus, as illustrated in Fig. 5a. These jacks are evenly distributed around the test specimen from 0° to 345° at 15° intervals along the horizontal plane. Vertically, four jacks are positioned at each specific angle: one jack acts on the upper ring, two on the middle ring, and one on the bottom ring. These jacks simulate the soil and water pressure exerted on the tunnel structure.

The ninety-six jacks are divided into three groups: P_1. P_2 and P_3[40]. All jacks within a group apply an identical force during each loading step. Twenty-four jacks near 0° and 180° are classified as P_1 to simulate vertical earth pressure. Forty jacks located near 90° and 270° are categorized as P_2 to simulate lateral earth pressure. The remaining thirty-two jacks, positioned near 45°, 135°, 225°, and 315°, are designated as P_3 to ensure a smooth transition of experimental load between P_1 and P_2.

The loading scheme for P_1. P_2 and P_3 are depicted in Fig. 5b. The tunnel specimen is assumed to be under a surcharge condition, which justifies the continuous increase of P_1. P_2 and P_3 during the experiment. The load scenario is potentially caused by construction activities above the tunnel, which is widely observed in actual

engineering practice and related research[14,23]. The design of these forces is based on the concept of minimizing the difference in internal forces between the experimental and actual loading conditions, as described in previous research[23,41]. For ease of the following discussion, the load magnitude descriptor $P=2\times(P_1-P_2)$ is defined[42], numerically representing the difference between the vertical and lateral earth pressure acting on a 1.2 m width of the tunnel structure, and indicating the magnitude of the asymmetric load borne by the tunnel.

The loading scheme is divided into two main phases. In the first phase, the unreinforced intact tunnel specimen is loaded until it reaches a predetermined damaged state, characterized by a structural convergence of 90 mm. At the end of this phase, SSCP reinforcement is applied to the tunnel specimen while maintaining the jack forces. In the second phase, after the reinforcement is completed, the experimental load continues to increase until the SSCP-reinforced tunnel reaches its ultimate bearing capacity. The timing for SSCP reinforcement is determined based on previous research[42], which shows that the tunnel structure enters the yielding stage at a convergence of 90 mm. At this point, the convergence rate accelerates, indicating the necessity for reinforcement. Furthermore, practical experience from Shanghai metro suggests that reinforcement should be applied when convergence reaches 80–100 mm.

Measurement program

Strain gauges and displacement meters are installed on the tunnel specimen, as shown in Fig. 6a. A total of 546 strain gauges are installed to measure the strain in the tunnel lining's rebar, concrete, bolts, and SSCP. A total of 67 displacement meters are installed to measure the structural convergence, joint opening, and joint misalignment.

For investigating the mechanical behavior of SSCP-reinforced tunnel structures, structural convergence, and SSCP strain are of primary interest, as depicted in Fig. 6b,c. Structural convergence, indicating overall tunnel deformation, is determined by the relative displacement between two points on the tunnel lining. Displacement meters for structural convergence are evenly spaced around the specimen at 45° intervals. SSCP strain gauges are placed on ten critical sections of the test specimen, including 0°, 90°, 270°, and stagger sections[42], where significant internal forces occur. The SSCP strain gauges are installed on both the crest and trough, as the SSCP features a sinusoidal wave pattern.

Failure mode

The structural convergence in the 90°-270°direction relative to the experimental load is shown in Fig. 7a. The points where the slope of the curve changes (①,②,③, and ④) are defined as structural performance points, marking the stages of damage progression within the tunnel structure.

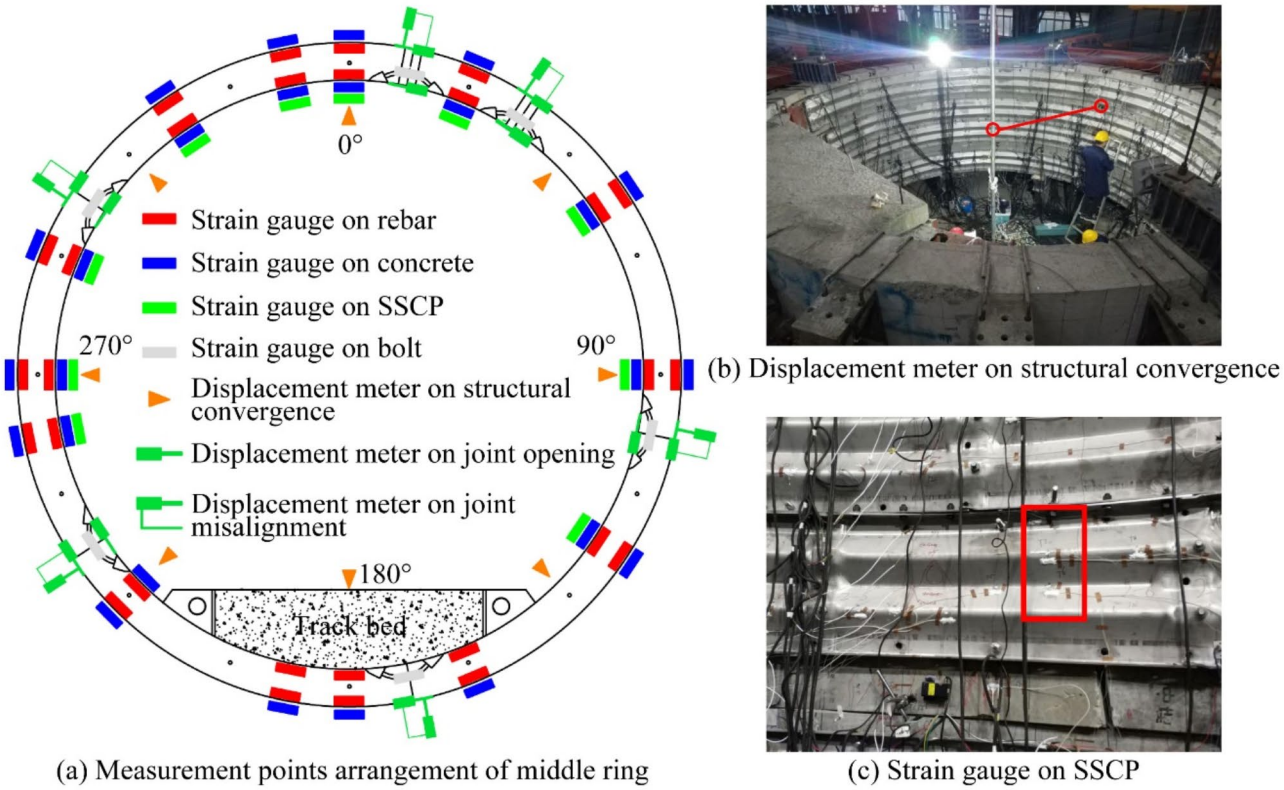

Fig. 6. Layout of measurement points (Reproduced with permission from Ka Gao, Ganshang Lu, and Jialiang Liu. We sincerely thank them for granting permission to use this image.)

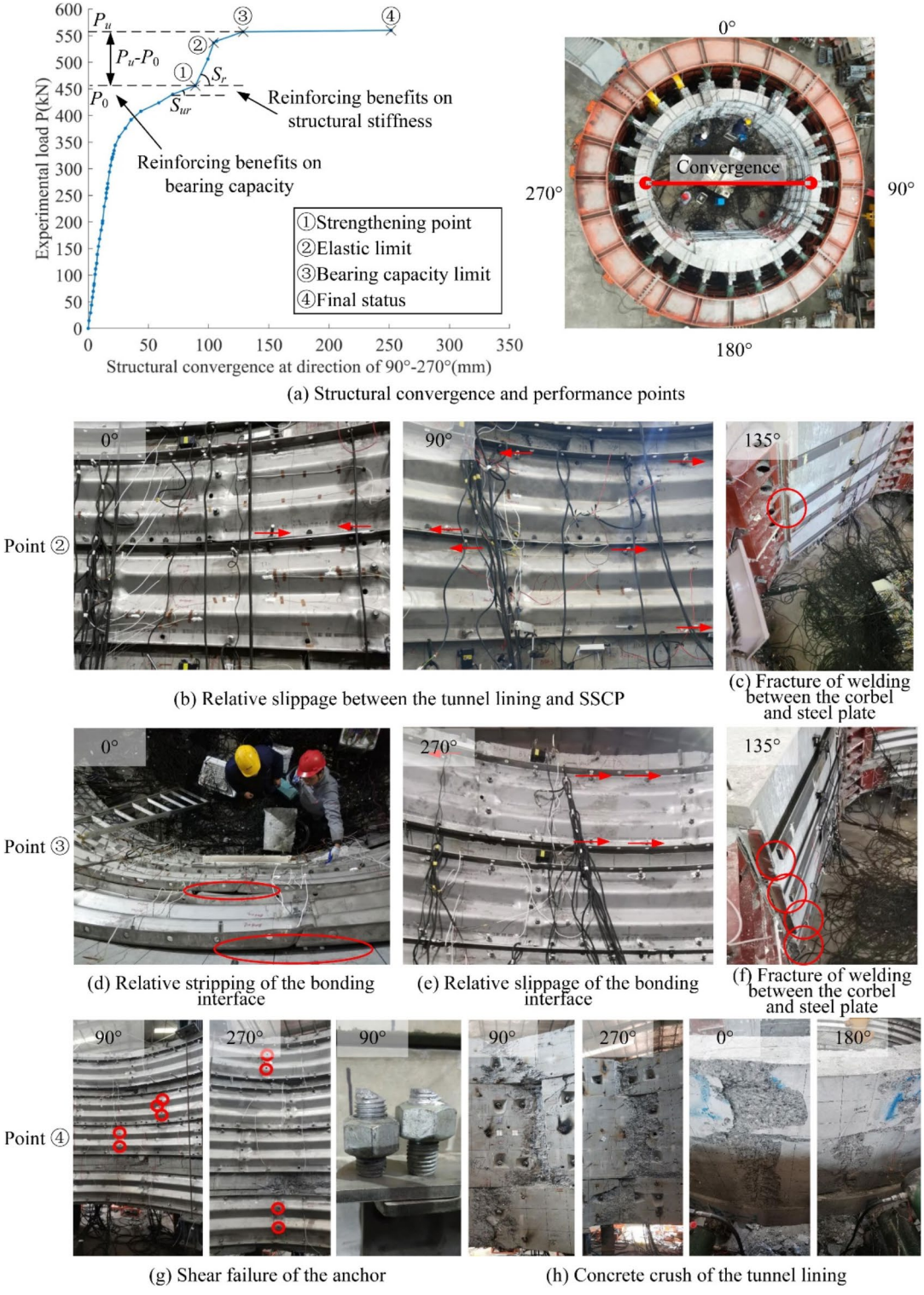

Fig. 7. Damage propagation and failure mode (Reproduced with permission from Ka Gao, Lei Xu, and Ganshang Lu. We sincerely thank them for granting permission to use this image.)

Before point ①, the unreinforced tunnel structure is loaded to a predetermined damaged state, exhibiting a convergence of 90 mm. As the load increases and damage accumulates, the slope of the structural convergence curve gradually decreases, indicating a reduction in structural stiffness. Theoretically, the tunnel structure reaches its bearing capacity when the slope of the structural convergence curve approaches zero, as the structure can no longer sustain additional load. Consequently, the continued decrease in slope also indicates the approach

to the structure's bearing capacity. For more details on the mechanical behavior of the unreinforced tunnel structure, please refer to our previous studies[41], as this paper focuses on the SSCP-reinforced tunnel structure.

Point ① represents the strengthening point, where SSCP reinforcement is applied to the damaged tunnel structure while maintaining a constant experimental load. The increase in slope after point ① reflects the reinforcing effects of SSCP on both structural stiffness and bearing capacity.

Point ② marks the elastic limit of the SSCP-reinforced structure, beyond which the slope of the structural convergence curve begins to decline. The phenomena observed at point ② are depicted in Fig. 7b,c. At this stage, relative slippage between the tunnel lining and SSCP becomes evident, indicating the onset of shear displacement at the bonding interface. Additionally, a fracture in the weld between the corbel and steel plate is observed, suggesting uncoordinated deformation between the corbel and track bed, particularly since the track bed, located at 180°, exhibits greater convergence than the corbel at 135°. However, this fracture is considered a localized damage with limited impact on the overall structural performance, as the uncoordinated deformation does not necessarily compromise the strength and stiffness of tunnel structure on the basis of structural mechanics.

Point ③ signifies the bearing capacity limit of the SSCP-reinforced structure, after which the slope of the structural convergence curve flattens to zero, indicating that the tunnel structure can no longer withstand additional external load. The phenomena observed at point ③ are shown in Fig. 7d–f. Significant relative stripping between the tunnel lining and SSCP is observed at 0°. Additionally, the relative slippage at the bonding interface continues to increase from point ② to ③ at 0°, 90° and 270°. Both the relative stripping and slippage reduce the compatibility of strain and stress at the bonding interface, weakening the collective load-bearing ability of the SSCP-reinforced structure, and ultimately leading to structural failure. Further fractures in the weld between the corbel and steel plate occur at point ③, though these are considered localized damages with limited impact on overall structural performance.

Point ④ represents the final state of the SSCP-reinforced structure, with corresponding phenomena illustrated in Fig. 7g,h. Shear failure of the anchors between the tunnel lining and SSCP is observed at 90° and 270°, where significant relative slippage occurs at the bonding interface, consistent with the previously discussed phenomena. The final condition of the tunnel lining is shown in Fig. 7h, where rapid concrete crushing occurs between points ③ and ④ due to the failure of the SSCP-reinforced structure.

In summary, the failure mode of the SSCP-reinforced tunnel structure is characterized by shear failure at the bonding interface, as evidenced by relative slippage at the interface and anchor shear failure. It is important to note that the bonding interface, exhibiting more significant stripping and slippage, is located near the longitudinal joints of the tunnel lining at the 0°, 90°, and 270° positions. According to our previous research[43], approximately 95% of the structural convergence is attributed to the rotation of the longitudinal joints, while the remaining 5% is due to the bending deformation of the concrete segments. As the loading progresses, the increasing structural convergence leads to greater rotations of the longitudinal joints, thereby inducing higher stress in the bonding interface at these locations. As a result, the bonding interface near the longitudinal joints is identified as a critical region where shear failure is most likely to occur.

Strengthening benefits

The experiment results offer valuable insights into the strengthening benefits of the SSCP-reinforced tunnel structure, as depicted in Fig. 7a. The strengthening benefits in structural bearing capacity are quantified by the difference in experimental load between the bearing capacity limit P_u and the strengthening point P_0, calculated as $(P_u\text{-}P_0)/P_0 = 22.15\%$. Similarly, the strengthening benefits in structural stiffness are assessed by the increase in the slope of the convergence curve before and after SSCP reinforcement, which is $(S_r\text{-}S_{ur})/S_{ur}=523\%$.

These findings demonstrated the effectiveness of SSCP reinforcement in enhancing the performance of shield tunnel structures, providing strong support for its practical application.

Measurement results of SSCP

Two SSCP rings are installed in the middle ring, as described in the previous section. The strain measurement results for these two SSCP rings are presented in Fig. 8.

The SSCPs exhibit higher strain at 0°, 90°, and 270°, which corresponds to locations of greater convergence and higher internal forces when the tunnel structure is subjected to a surcharge condition. The SSCPs tend to resist the increase in convergence by absorbing internal forces at those locations, leading to elevated strain levels in the SSCPs.

At structural performance point ③, the maximum strain in the SSCPs is 806με, which is well below 2000με. This indicates the strength of the SSCP material is not fully utilized when the tunnel structure reaches its bearing capacity. This underutilization occurs because the failure of the SSCP-reinforced structure is governed by shear failure at the bonding interface. The shear force transferred across the bonding interface plays a crucial role in SSCP reinforcement by enabling a shared load-bearing mechanism between the newly installed SSCPs and the tunnel linings. This mechanism significantly enhances the structural bearing capacity and stiffness. However, as the structural failure is initiated by shear failure at the bonding interface rather than the material failure of the SSCPs, the full strength of the SSCP material remains underutilized, leaving residual strength in the SSCPs, as illustrated in Fig. 8.

A detailed examination of the strain distribution at structural performance point ④ reveals several discrepancies. Firstly, the strain levels between the two rings at the same angle differ significantly. For example, at 0°, SSCP ring 1 experiences a strain of 438με, while SSCP ring 2 experiences 2645με. Secondly, within the same SSCP ring, adjacent SSCPs exhibit large discrepancies in strain. In SSCP ring 2, the strain at 0° is 2645με, while the adjacent SSCP shows nearly zero strain at 350°. These discrepancies are attributed to the limited connecting stiffness between the SSCPs. Adjacent SSCPs within a single ring are connected by only three bolts, and there

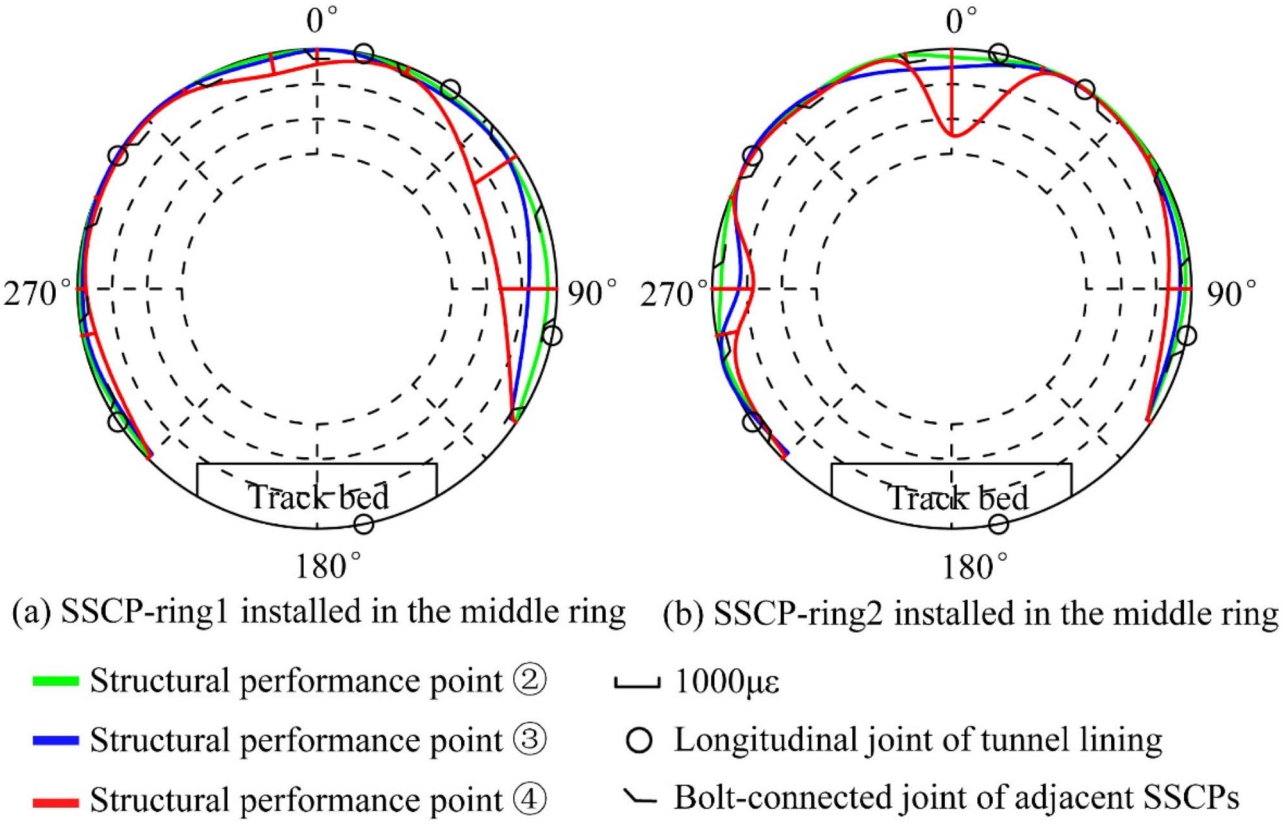

Fig. 8. Absolute maximum value of SSCP strain at various structural performance points.

is no connection between the two SSCP rings. This insufficient connecting stiffness impedes the strain transfer between SSCPs, thereby reducing their collective load-bearing capacity and undermining the overall reinforcing benefits of the SSCPs.

Proposed design concepts

Design concepts are proposed based on experimental observations, serving as a bridge between academic research and engineering practice, and providing guidelines for practical application.

Concept a Enhancing interface bonding shear strength.

Shear failure of the bonding interface is identified as the primary failure mode of SSCP-reinforced tunnel structures. Furthermore, SSCP material strength remains underutilized when this shear failure occurs, as indicated by the strain analysis. By increasing the bonding shear strength at the interface, the onset of interface failure can be delayed, allowing for better utilization of the SSCP material strength, thereby enhancing the overall structural bearing capacity. Similarly, previous research indicates that the bonding strength between the reinforcement material and the tunnel lining is critical for enhancing the ultimate capacity of reinforced composite structures[44,45].

Concept B Improving connecting stiffness between SSCPs.

Experiment results reveal that inadequate connecting stiffness between SSCPs hinders the reinforcing benefits of the SSCPs. It is recommended to increase the connecting stiffness both between adjacent SSCPs within a single ring and between SSCP rings. This would enable the SSCPs to collectively bear external loads as a continuous ring, thereby offering superior reinforcement benefits. Similarly, previous research employs welding between adjacent steel plates to ensure the structural integrity of the reinforced tunnel structure.

Practical implementation

This section outlines the practical implementation of SSCP reinforcement, including the SSCP layout, application of design concepts, construction process, and an evaluation of construction and economic efficiency, offering valuable insights for future applications.

Layout of SSCP reinforcement

Three SSCP rings, each 460 mm wide, are installed on a single 1600 mm wide ring of the tunnel lining (Fig. 9b). Each SSCP ring is composed of fourteen SSCPs with an arc length of either 1191.7 or 1354.7 mm (Fig. 9a). Adjacent SSCPs within a ring are connected by five bolts through longitudinal bolt holes. The SSCP rings themselves are connected by bolts spaced 159.5 mm apart along the arc, using circumferential bolt holes. The SSCPs are anchored to the tunnel lining with an implantation depth of 160 mm. Both the bolts and anchors are made of 2205 stainless steel, with a diameter of 16 mm. The bonding interface between the SSCPs and the tunnel lining is filled with mortar, which provides tensile and shear strengths of 2.5 MPa and 17 MPa, respectively.

In this case study, the SSCP rings are connected directly to a steel plate at the bottom of the tunnel lining (Fig. 9a), differing from the experimental specimen, where they are connected to corbels on either side of the track bed, which are further linked by steel plates. Directly connecting the SSCP rings to the bottom steel plate

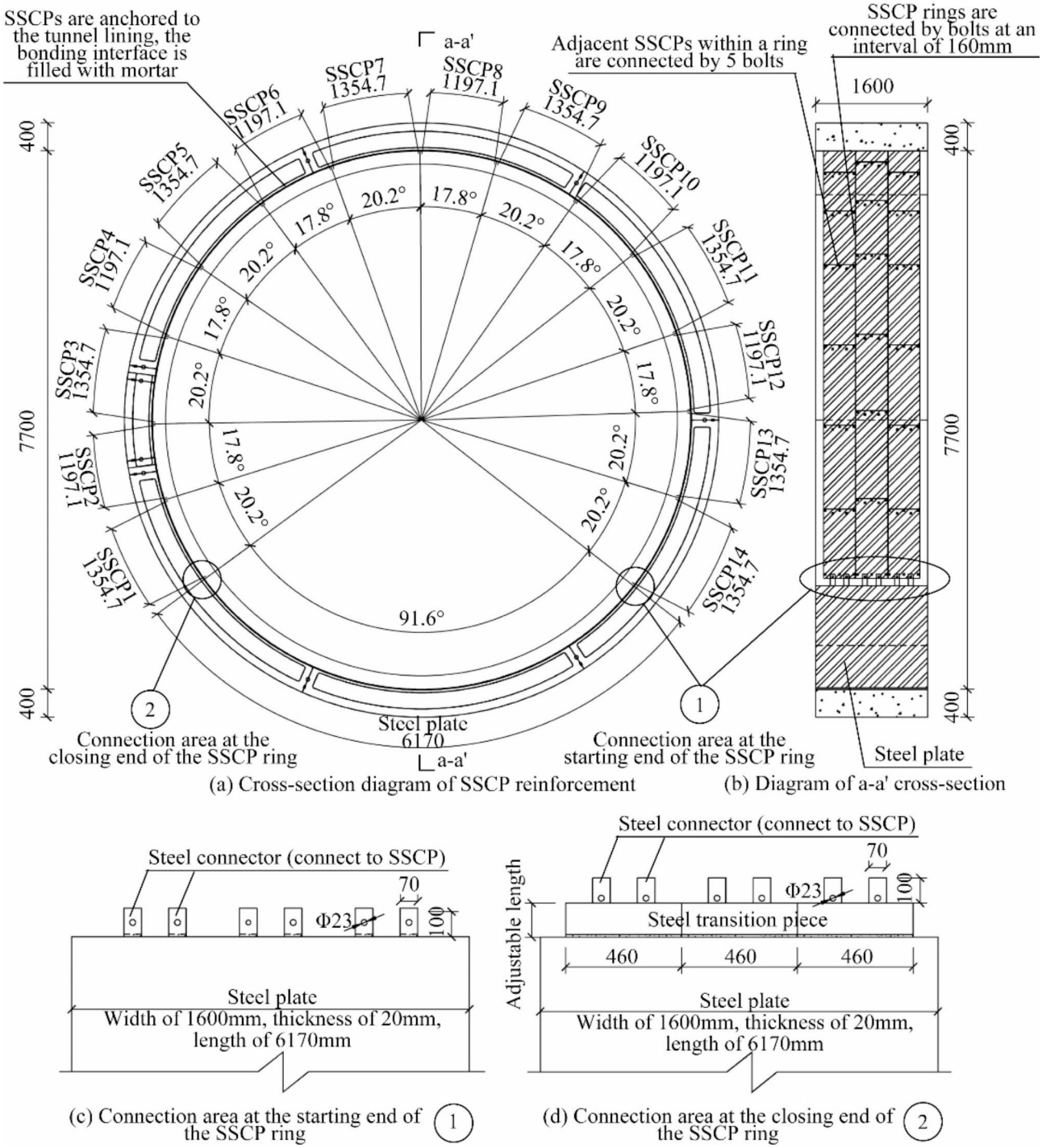

Fig. 9. Geometric layout of SSCP reinforcement.

allows for better-coordinated deformation across the entire ring, avoiding the weld fractures between the corbel and the steel plate caused by uncoordinated deformation—an issue observed in the experiment and discussed in the previous section. Additionally, in this case study, SSCP reinforcement is conducted before casting the track bed, facilitating this reinforcement layout. The bottom steel plate is made of Q345B steel, with dimensions of 1600 mm in width, 6170 mm in arc length, and 20 mm in thickness.

The connection areas between the SSCP rings and the bottom steel plate are illustrated in Fig. 9c,d, which include the starting and closing ends. At the starting end, steel connectors are welded to the bottom steel plate. These connectors are 70 mm wide, 100 mm high, 20 mm thick and have bolt holes with a diameter of 23 mm. The first-installed SSCP is bolted to the bottom steel plate through these bolt holes. At the closing end, the last-installed SSCP is similarly bolted to the bottom steel plate by steel connectors, but with an additional steel transition piece welded between the connectors and the bottom steel plate. The steel transition piece is 1380 mm wide, with an adjustable length to accommodate installation deviations of the SSCP rings. It is important to avoid welding directly on the SSCPs, as they are made of stainless steel, which can experience material property degradation from welding.

Application of design concepts

It should be noted that the design concepts proposed in the previous section are applied in this practical implementation (Fig. 10).

Regarding the concept of enhancing interface bonding shear strength, mortar is used to fill the bonding interface between the tunnel lining and SSCPs. The total tensile and shear strength of the bonding interface is provided by both the mortar and the anchors. The strength can be quantified by multiplying the material strength by the effective area that provides resistance. Given that the mortar offers a larger effective area compared to the anchors, it contributes more to the tensile and shear strength of the bonding interface. By filling the bonding interface with mortar, the interface's strength is increased, delaying the onset of shear failure and thereby enhancing the bearing capacity of the SSCP-reinforced structure.

For the concept of improving connecting stiffness between SSCPs, both the longitudinal and circumferential connections between the SSCPs are improved by increasing the number of bolts. The number of bolts connecting adjacent SSCPs within a ring is increased from three to five, compared to the experimental specimen. Additionally, two SSCP rings are now connected by bolts spaced 159.5 mm apart along the arc, a connection that is absent in the experiment. Bolts are made of 2205 stainless steel with a diameter of 16 mm. By enhancing the connecting stiffness between SSCPs, the SSCPs can collectively bear external loads as a continuous ring, resulting in greater structural stiffness in the SSCP-reinforced structure.

To further enhance the strengthening benefits, a method aside from the two design concepts mentioned above involves planting additional steel bars at the longitudinal joints to better connect adjacent concrete segments. This method helps control joint opening, which is essential for mitigating shear failure at the bonding interface. As discussed in Sect. 3.2, shear failure typically begins at the longitudinal joints due to the substantial rotation of these joints under loading. By introducing additional steel bars, the rotation of the longitudinal joints can be restrained, thereby delaying the onset of shear failure at the bonding interface. Although this method was not applied in the practical implementation of this study due to its time-consuming nature, the authors consider it a viable approach for enhancing the strengthening benefits, particularly in severely deformed tunnels.

The technical details regarding the design concepts are listed as follows:

(1) A pre-assembly test should be conducted before on-site installation[19].

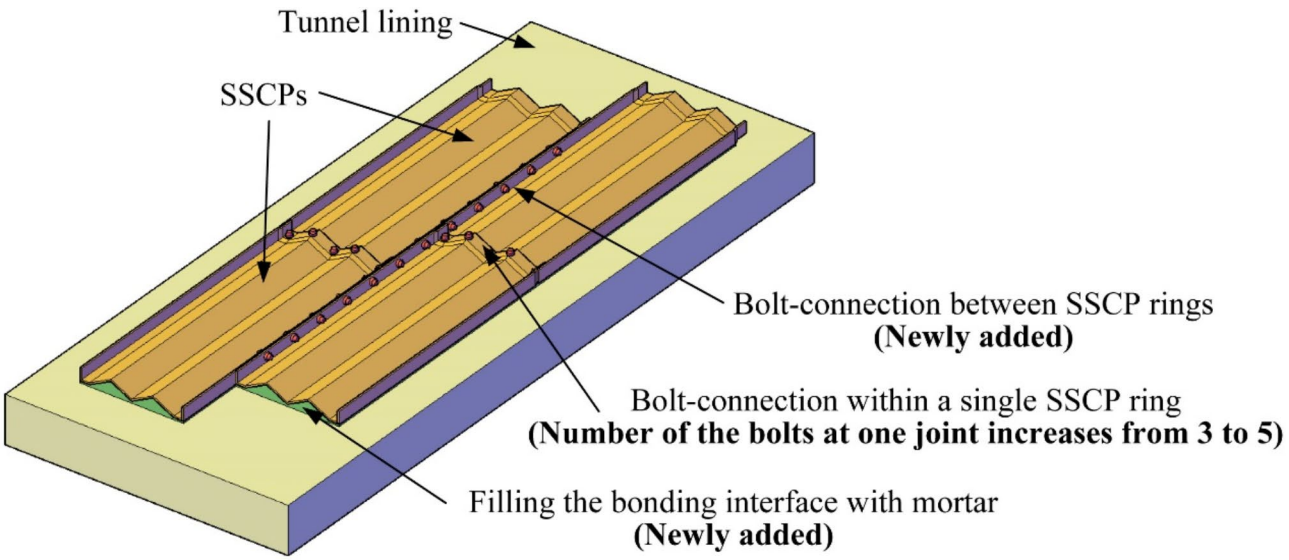

Fig. 10. Scheme on application of design concepts.

(2) The alignment deviation between SSCPs is set to be within 1 mm for a single ring and 5 mm between rings[46,47].

(3) The gap between the outer side of the SSCP and the inner side of the tunnel lining should be kept below 20 mm[19].

(4) Any dust or debris in the gap between the SSCP and the tunnel lining should be thoroughly cleaned before filling with mortar[18,19].

(5) An inspection method, such as percussion testing, should be used to assess the uniformity of mortar.

Points (1) and (2) ensure greater precision and accuracy in installation, thereby improving the connecting stiffness between SSCPs. Points (3) and (4) facilitate higher-quality mortar filling, enhancing the interface bonding shear strength.

Construction process

The construction process for SSCP reinforcement is outlined in Fig. 11.

(1) Preparation: The first step involves sealing where concrete has been crushed, as well as the longitudinal joints and bolt hand holes, using cement mortar. This prevents mortar from leaking out through these gaps during the subsequent filling of the bonding interface.

(2) Reinforcement installation: Before on-site installation, a pre-assembly test is conducted. By assembling an SSCP ring in a controlled environment before on-site installation, alignment issues can be identified and addressed in advance. This proactive step helps optimize the installation process and reduces the risk of misalignments during on-site assembly. During the on-site installation, the bottom steel plate is installed first, providing support for the SSCPs. The steel connector at the starting end, which links the bottom steel plate to the first SSCP, is welded to the plate's edge. The first SSCP is then bolted to this connector. Subsequent SSCPs are installed sequentially from the starting to the closing end, with bolt connections made between adjacent SSCPs and anchors planted between the SSCPs and the tunnel lining. Before installing the final SSCP, a trail

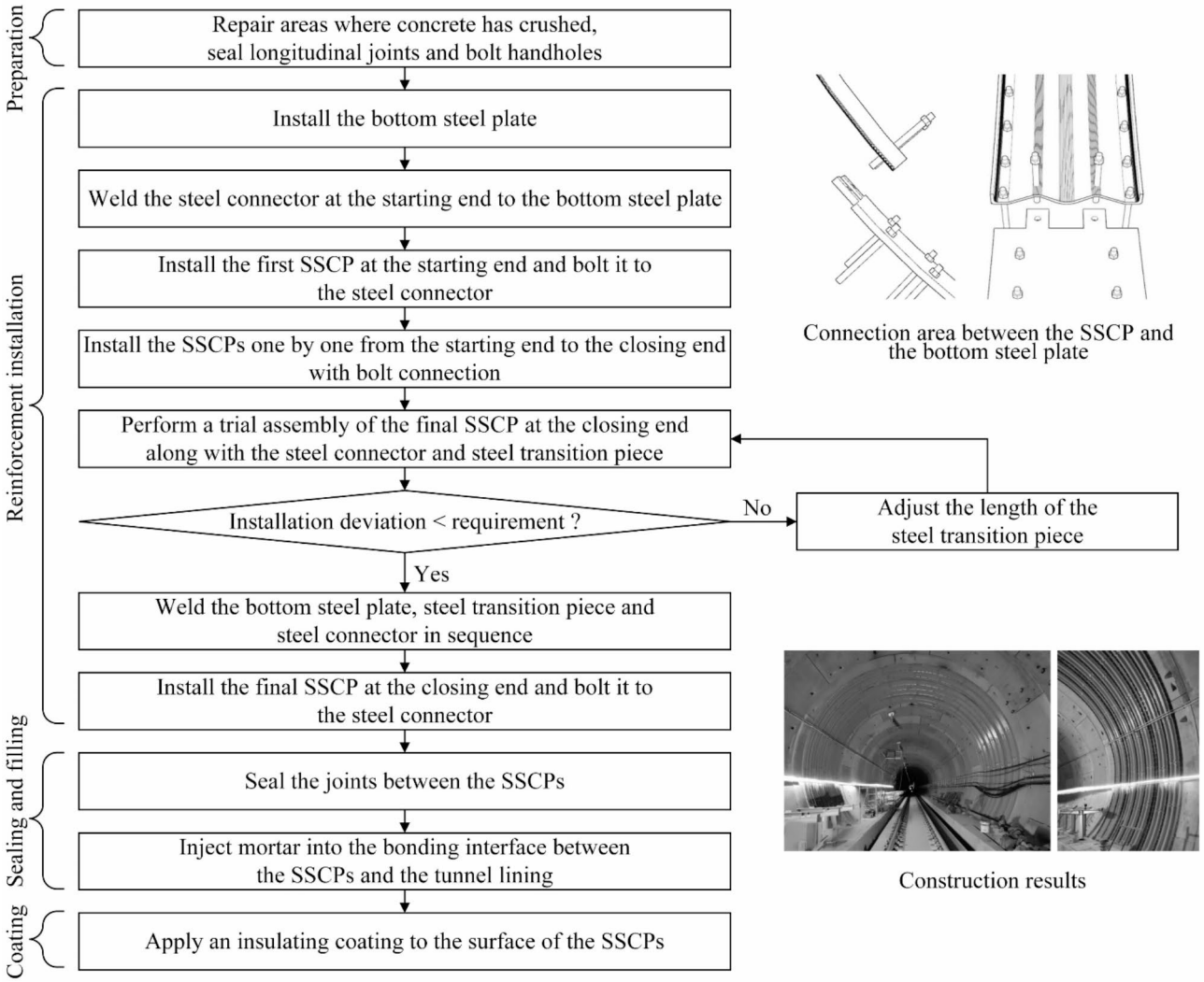

Fig. 11. Construction process of SSCP reinforcement.

assembly is conducted at the closing end with the steel connector and the steel transition piece. The length of the steel transition piece is adjusted during this trial to meet the installation tolerance requirements. Once the adjustments are completed, the bottom steel plate, steel transition piece, and steel connector are welded in sequence, and the final SSCP is installed. In summary, the use of pre-assembly and trial assembly techniques mitigates gaps and misalignments between SSCPs, ensuring a smoother on-site assembly process.

(3) Sealing and filling: The joints between the SSCPs are sealed with cement mortar, similar to the earlier sealing of longitudinal joints and bolt hand holes. Mortar is then injected into the bonding interface through a designated hole at the top of the SSCP ring. There are two such holes on the SSCP rings: one for filling with mortar and the other for venting air from the interface, reducing air bubbles and ensuring better filling quality.

(4) Coating application: Finally, an anti-corrosion coating is applied to the bottom steel plate, and an insulating coating is applied to both the bottom steel plate and the SSCPs. Since the SSCPs are made of stainless steel, they do not require anti-corrosion coating. The insulating coating is applied to prevent stray currents that could arise during future operations.

The final results of the construction are shown in the bottom-left corner of Fig. 11.

Discussion

Construction efficiency

To evaluate the construction efficiency of SSCP reinforcement, its duration and labor requirements are analyzed (Fig. 12). The construction process involves a team of ten workers operating at a standard pace of eight hours per day. SSCP reinforcement is completed in 13 days, demonstrating notable efficiency.

This efficiency is primarily attributed to two factors: the simplified installation process and reduced coating requirements. The installation of SSCPs uses bolt connections, which are faster and require less specialized labor compared to conventional steel plate reinforcement method. Additionally, the lighter weight of SSCPs simplifies transportation and handling, reducing setup time and the number of workers needed. Furthermore, SSCPs only require an insulating coating due to their stainless steel composition, which offers excellent corrosion resistance. This eliminates the need for anti-corrosion coatings, saving additional time during the coating process. These advantages collectively emphasize the construction efficiency of SSCP reinforcement in shield tunnel applications.

Economic efficiency

The economic efficiency of SSCP reinforcement is compared to that of steel plate reinforcement using the metric of steel usage pre-unit area for tunnel reinforcement (Fig. 13). This metric measures the weight of steel used per square meter of tunnel lining surface. SSCP reinforcement requires 63.2 kg/m^2 of steel, which is 60% less than the 158 kg/m^2 needed for steel plate reinforcement, demonstrating the superior economic efficiency of SSCP reinforcement.

It is important to note that the moment of inertia transverse to the corrugation direction of the SSCP is $8.43 \times 10^7 mm^4$, nearly 300 times greater than the $3.07 \times 10^5 mm^4$ of steel plate reinforcement with the same width. This means SSCP reinforcement uses fewer materials while providing significantly greater stiffness to the tunnel structure.

Furthermore, the superior economic efficiency of SSCP reinforcement can be demonstrated through a lifecycle cost evaluation, which considers the project's total cost over its entire lifespan. This evaluation mainly includes the initial installation costs and ongoing maintenance costs.

In terms of material costs, SSCP does have slightly higher expenses due to the cost of filling materials. However, SSCP shows significant cost advantages in other areas. Labor and equipment costs are reduced with SSCP due to its simplified installation process, which does not require heavy machinery or complex welding. Maintenance costs, including re-coating expenses, are notably lower for SSCP-reinforced structures. SSCP's superior corrosion resistance means that maintenance is required less frequently compared to conventional steel plate reinforcements.

The lifecycle cost evaluation shows that while SSCP may have slightly higher initial filling material costs, it offers significant savings in the long term. Reduced labor and maintenance costs make SSCP a more economically efficient solution for tunnel reinforcement.

In summary, SSCP reinforcement offers greater construction and economic efficiency compared to conventional steel plate reinforcement, highlighting its promising potential for practical implementation.

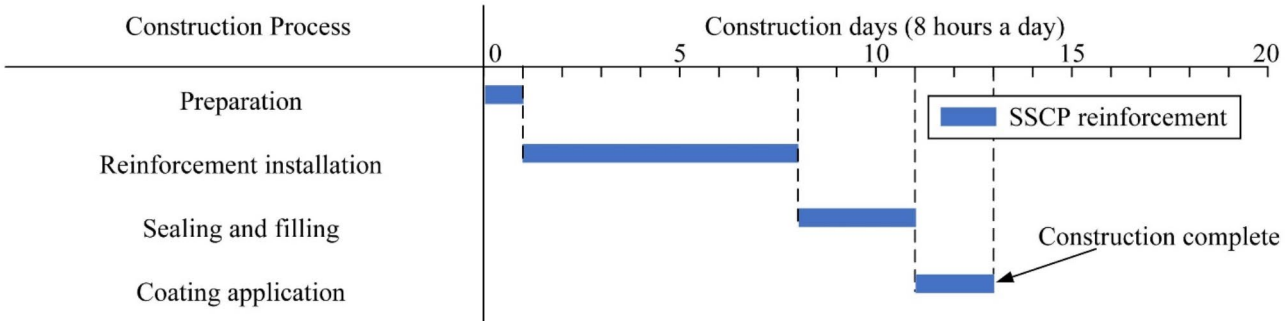

Fig. 12. Construction efficiency of SSCP reinforcement.

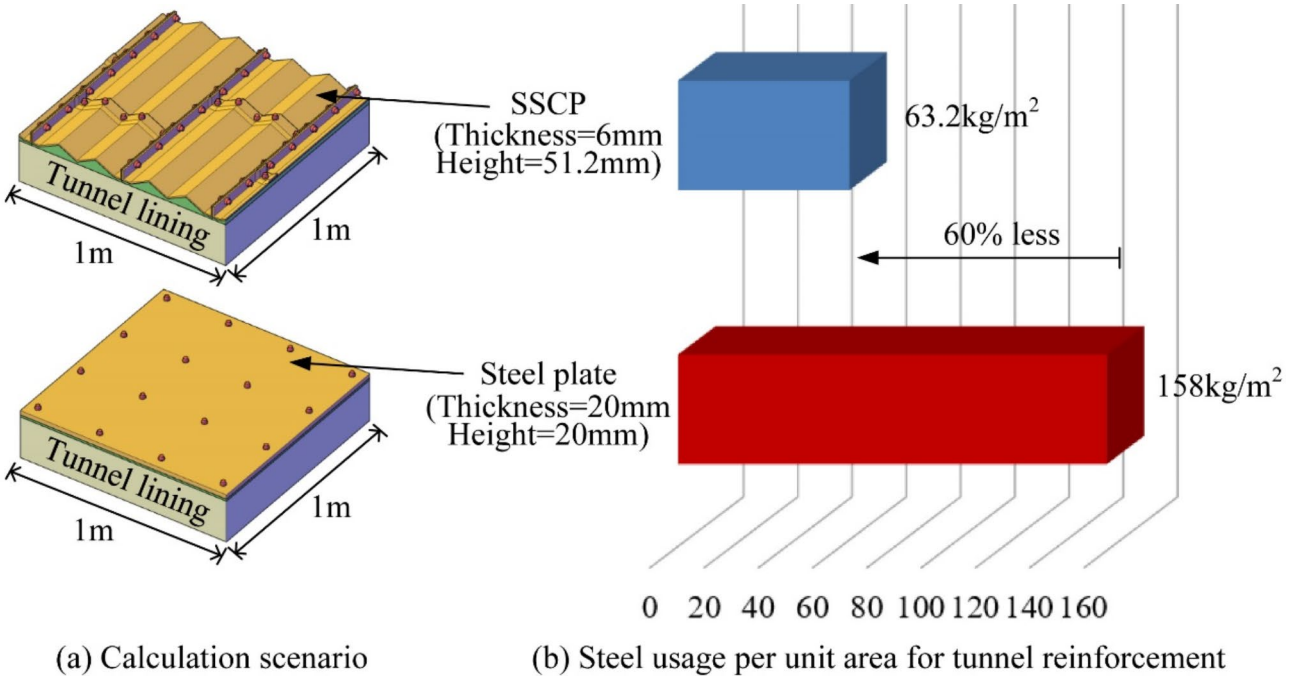

Fig. 13. Comparison of economic efficiency between SSCP and steel plate reinforcement.

Conclusions

This paper presents a case study on the reinforcement of an impaired shield tunnel structure using SSCP, offering valuable insights for both academic research and engineering practice:

(1) Academic insights: Experimental results confirm that SSCP reinforcement effectively enhances both the structural bearing capacity and stiffness of the tunnel. Additionally, the failure mode of the SSCP-reinforced tunnel structure is identified as shear failure at the bonding interface, evidenced by relative slippage at the interface and anchor shear failure.

(2) Design concepts: Two design concepts are proposed based on experimental observations, bridging academic research and engineering practice: enhancing interface bonding shear strength and improving connecting stiffness between SSCPs. The first concept delays interface failure, allowing for better utilization of the SSCP material strength, thereby improving structural bearing capacity. The second concept enables SSCPs to bear external loads collectively as a continuous ring, resulting in superior reinforcement benefits.

(3) Practical implications: SSCP reinforcement demonstrates greater construction and economic efficiency compared to conventional steel plate reinforcement. Particularly, it is suggested to use SSCP reinforcement in shield tunnels with high utilization rates and humid environments. According to the experimental results, it is recommended to fill the bonding interface with high-strength mortar and install additional bolts between adjacent SSCPs to enhance the mechanical performance of the SSCP-reinforced tunnel structure.

Data availability

The data used during this study is available from the corresponding author upon reasonable request.

Received: 24 December 2024; Accepted: 10 March 2025
Published online: 09 April 2025

References

1. China Association of Metros. *2023 Annual Report of China Urban Mass Transit* Vol. 57 1–14. (in Chinese). (China Association of Metros, 2024).
2. Liu, T. J., Chen, S. W. & Liu, H. Y. Deformation characterisation and distress diagnosis of a metro shield tunnel by adjacent constructions. *Adv. Civ. Eng.* 4216349 (2020).
3. Liu, D. et al. Structural responses and treatments of shield tunnel due to leakage: A case study. *Tunn. Undergr. Space Technol.* **103**, 103471 (2020).
4. Yuan, B., Liang, J., Lin, H., Wang, W. & Xiao, Y. Experimental study on influencing factors associated with a new tunnel waterproofing for improved impermeability. *J. Test. Eval.* **52**, JTE20230417 (2024).
5. Huang, Z., Fu, H., Chen, W., Zhang, J. & Huang, H. Damage detection and quantitative analysis of shield tunnel structure. *Autom. Constr.* **94**, 303–316 (2018).
6. Cui, H., Ren, X., Mao, Q., Hu, Q. & Wang, W. Shield subway tunnel deformation detection based on mobile laser scanning. *Autom. Constr.* **106**, 102889 (2019).
7. Huang, H., Zhao, S., Zhang, D. & Chen, J. Deep learning-based instance segmentation of cracks from shield tunnel lining images. *Struct. Infrastruct. Eng.* **18**, 183–196 (2022).

8. Han, W. et al. Review of health inspection and reinforcement design for typical tunnel quality defects of voids and insufficient lining thickness. *Tunn. Undergr. Space Technol.* **137**, 105110 (2023).
9. Wang, J. H. Lifecycle cost and performance analysis for repair of concrete tunnels. In *Eco-efficient Repair and Rehabilitation of Concrete Infrastructures* 637–672 (Woodhead Publishing, 2018).
10. Wei, G. et al. Experiments and numerical simulation of the reinforcement effect of channel-steel-reinforced shield tunnel segments under unloading conditions. *Eur. J. Environ. Civ. Eng.* **27**, 4142–4164 (2023).
11. Liu, X., Jiang, Z. & Zhang, L. Experimental investigation of the ultimate bearing capacity of deformed segmental tunnel linings strengthened by epoxy-bonded filament wound profiles. *Struct. Infrastruct. Eng.* **13**, 1268–1283 (2017).
12. Li, L., Khan, M., Jiang, X., Shakor, P. & Zhang, Y. Sustainable fiber reinforced cementitious composites for construction and Building materials. *Front. Mater.* **10**, 1237960 (2023).
13. Chen, R. P. et al. Experimental study on the mechanical behavior of segmental joints of shield tunnels strengthened by a steel plate-UHPC composite. *Tunn. Undergr. Space Technol.* **144**, 105536 (2024).
14. Liu, T. J., Chen, S. W., Lin, P. Q. & Liu, H. Y. Failure mechanism and strengthening effect of shield tunnel lining reinforced by steel plates with corbels. *Eur. J. Environ. Civ. Eng.* **26**, 1603–1621 (2022).
15. Li, Z., Liu, X., Lai, H., Yang, Z. & Wang, B. Detailed damage mechanism of deformed shield tunnel linings reinforced by steel plates. *Eng. Fail. Anal.* **143**, 106850 (2023).
16. Liu, D., Wang, F., Zhang, D. & Duan, K. Interfacial stresses of shield tunnel strengthened by a thin plate at inner surface. *Tunn. Undergr. Space Technol.* **91**, 103021 (2019).
17. Zhang, D. M., Zhai, W. Z., Huang, H. W. & Chapman, D. Robust retrofitting design for rehabilitation of segmental tunnel linings: using the example of steel plates. *Tunn. Undergr. Space Technol.* **83**, 231–242 (2019).
18. Chen, H., Lai, H., Qiu, Y. & Chen, R. Reinforcing distressed lining structure of highway tunnel with bonded steel plates: case study. *J. Perform. Constr. Facil.* **34**, 04019082 (2020).
19. Zhang, Y. et al. Failure of urban subway segments in coastal area and reinforcement effect of bonded steel plate: a case study in China. *Struct. Infrastruct. Eng.* 1–13 (2023).
20. Li, S., Ding, W., Zhang, Q., Xiao, X. & Zhou, Q. Experimental study of the mechanical properties of a new duplex stainless steel exposed to elevated temperatures. *Case Stud. Constr. Mater.* **17**, e01683 (2022).
21. Bautista, A., Velasco, F. & Torres-Carrasco, M. Influence of the alkaline reserve of chloride-contaminated mortars on the 6-year corrosion behavior of corrugated UNS S32304 and S32001 stainless steels. *Metals* **9**, 686 (2019).
22. Myslicki, S. et al. Fatigue of glued-in rods in engineered hardwood products—Part I: experimental results. *J. Adhes.* **95**, 675–701 (2019).
23. Liu, X., Jiang, Z., Yuan, Y. & Mang, H. A. Experimental investigation of the ultimate bearing capacity of deformed segmental tunnel linings strengthened by epoxy-bonded steel plates. *Struct. Infrastruct. Eng.* **14**, 685–700 (2018).
24. Li, Q. et al. Long-term corrosion monitoring of carbon steels and environmental correlation analysis via the random forest method. *npj Mater. Degrad.* **6**, 1 (2022).
25. Zhao, G., Song, R., He, B., Meng, S. & Zhou, X. Mechanical properties and damage mechanism of corrugated steel plate–concrete composite structures as primary supports of tunnels. *Constr. Build. Mater.* **449**, 138389 (2024).
26. Ding, W., Guo, Y., Li, S., Li, X. & Zhang, Q. Experimental research on the mechanical behavior of segmental joints of shield tunnel reinforced with a new stainless steel corrugated plate. *Case Stud. Constr. Mater.* **18**, e02170 (2023).
27. Zhao, G., Liu, J., Meng, S., Liu, C. & Wang, Q. Performance of corrugated steel plate flange joint under combined compression and bending: experimental and numerical investigations. *Constr. Build. Mater.* **389**, 131798 (2023).
28. Ren, T., Liu, S. & Liu, X. Experimental study of bearing capacity of shield tunnel lining segment strengthened by corrugated steel. *Tunn. Constr.* **39**, 317–323 (2019).
29. Liang, K. et al. Failure mechanism of underwater shield tunnel: an experimental and theoretical study. *Tunn. Undergr. Space Technol.* **137**, 105155 (2023).
30. Liu, X., Dong, Z., Bai, Y. & Zhu, Y. Investigation of the structural effect induced by stagger joints in segmental tunnel linings: first results from full-scale ring tests. *Tunn. Undergr. Space Technol.* **66**, 1–18 (2017).
31. Xu, P., Wei, Y., Yang, Y. & Zhou, X. Application of fabricated corrugated steel plate in subway tunnel supporting structure. *Case Stud. Constr. Mater.* **17**, e01323 (2022).
32. Niu, Y. et al. Research on bearing behaviour of buried double corrugated steel culvert with high fill considering spacing effect. *Case Stud. Constr. Mater.* **20**, e02943 (2024).
33. Amjad, R., Zhang, Y. & Liu, X. An analytical solution for shear bearing capacity of circumferential joints of precast concrete segmental tunnel linings considering dowel action. *Struct. Concr.* **25**, 4918–4937 (2024).
34. Zhang, X. et al. Monitoring-assisted large-diameter shield tunneling control in soft ground: A case study of bund tunnel project. In *Eighth International Conference on Case Histories in Geotechnical Engineering* 306–314 (American Society of Civil Engineers, 2019).
35. Chen, H. et al. Shield attitude prediction based on Bayesian-LGBM machine learning. *Inf. Sci.* **632**, 105–129 (2023).
36. Li, X., Lin, X., Zhu, H., Wang, X. & Liu, Z. Condition assessment of shield tunnel using a new indicator: the tunnel serviceability index. *Tunn. Undergr. Space Technol.* **67**, 98–106 (2017).
37. Xie, X., Yang, Y. & Ji, M. Analysis of ground surface settlement induced by the construction of a large-diameter shield-driven tunnel in Shanghai, China. *Tunn. Undergr. Space Technol.* **51**, 120–132 (2016).
38. GB 50010 – 2010. *Code for Design of Concrete Structures* (China Building Industry, 2010) (**in Chinese**).
39. GB 50017 – 2017. *Code for Design of Steel Structures* (China Building Industry, 2017) (**in Chinese**).
40. Zhang, L. & Liu, X. Experimental investigation of the deformed stagger-jointed segmental tunnel linings strengthened by epoxy-bonded filament wound profiles. *Materials* **15**, 6862 (2022).
41. Liu, X., Bai, Y., Yuan, Y. & Mang, H. A. Experimental investigation of the ultimate bearing capacity of continuously jointed segmental tunnel linings. *Struct. Infrastruct. Eng.* **12**, 1364–1379 (2016).
42. Liu, X., Zhang, Y. & Bao, Y. Full-scale experimental investigation on stagger effect of segmental tunnel linings. *Tunn. Undergr. Space Technol.* **102**, 103423 (2020).
43. Zhang, J. L., Mang, H. A., Liu, X., Yuan, Y. & Pichler, B. On a nonlinear hybrid method for multiscale analysis of a bearing-capacity test of a real-scale segmental tunnel ring. *Int. J. Numer. Anal. Methods Geomech.* **43**, 1343–1372 (2019).
44. Chang, C. T., Wang, M. J., Chang, C. T. & Sun, C. W. Repair of displaced shield tunnel of the Taipei rapid transit system. *Tunn. Undergr. Space Technol.* **16**, 167–173 (2001).
45. Zhao, H., Liu, X., Bao, Y., Yuan, Y. & Bai, Y. Simplified nonlinear simulation of shield tunnel lining reinforced by epoxy bonded steel plates. *Tunn. Undergr. Space Technol.* **51**, 362–371 (2016).
46. DG/TJ 08-2231-2017. *Code for Acceptance of Construction Quality of Repair and Reinforcement Engineering for Subway Shield Tunnel* (Tongji University, 2017). (**in Chinese**).
47. Kiriyama, K. et al. Structure and construction examples of tunnel reinforcement method using thin steel panels. *Nippon Steel Tech. Rep.* **92**, 45–50 (2005).

Acknowledgements
This research was funded by the State Grid Corporation of China science and technology project "Research and Application of Key Technology for Online Monitoring of Transmission Pipeline Corridor Structural Health Status Based on Fiber Optic Micro- and Nanoscale Measurements" (grant number 5700–202313621 A-3-2-ZN).

Author contributions
Yimin Qin: methodology, investigation, writing - original draft, and, visualization. Yizheng Chen: conceptualization, resources, writing - review & editing, and, funding acquisition. Yan Tang: methodology, investigation, and, visualization. Cheng Zhong: methodology and investigation. Shurong Li: investigation. Xian Liu: conceptualization, writing - review & editing, and, supervision. All authors reviewed the manuscript.

Declarations

Competing interests
The authors declare no competing interests.

Additional information
Correspondence and requests for materials should be addressed to Y.C. or X.L.

Reprints and permissions information is available at www.nature.com/reprints.

Publisher's note Springer Nature remains neutral with regard to jurisdictional claims in published maps and institutional affiliations.